Supplementary Information to:

“Decadal-to-centennial increases of volcanic aerosols from Iceland challenge the concept of a Medieval Quiet Period”

Imogen Gabriel[1], Gill Plunkett[2], Peter M. Abbott[1], Melanie Behrens[3], Andrea Burke[4], Nathan Chellman[5], Eliza Cook[6], Dominik Fleitmann[7], Maria Hörhold[3], William Hutchison[4], Joseph R. McConnell[5], Bergrún A. Óladóttir[8], Johannes Preiser-Kapeller[9], Jakub T. Sliwinski[4], Patrick Sugden[4], Birthe Twarloh[3], and Michael Sigl[1,10]

1 Climate and Environmental Physics & Oeschger Centre for Climate Change Research, University of Bern, 3012 Bern, Switzerland

2 Archaeology & Palaeoecology, School of Natural and Built Environment, Queen’s University Belfast, Belfast BT7 1NN, UK

3 Alfred-Wegener-Institut Helmholtz-Zentrum für Polar- und Meeresforschung, 27570 Bremerhaven, Germany

4 School of Earth and Environmental Sciences, University of St Andrews, St Andrews KY16 9TS, UK

5 Desert Research Institute, Nevada System of Higher Education, Reno, Nevada 89512, USA

6 Physics of Ice, Climate and Earth, Niels Bohr Institute, University of Copenhagen, 2200 Copenhagen, Denmark

7 Department of Environmental Sciences, University of Basel, 4056 Basel, Switzerland

8 Icelandic Meteorological Office, 150 Reykjavík, Iceland

9 Department of Byzantine Research/Institute for Medieval Research, Austrian Academy of Sciences, A-1010 Vienna, Austria

10 Department of Geosciences, University of Oslo, 0371 Oslo, Norway

I. Supplementary Methods

A) *Summary of the Ice-core cryptotephra sample preparation methodology for geochemical analysis at the University of Bern adopted within this study.*

Subsampling. Samples of varying lengths (between 5cm and 13cm) were obtained for each event following the adoption of a targeted sampling strategy. The length of the sample was based on the ice core glaciochemical records (non-sea-salt sulfur and insoluble particle records) which were used to assist in isolating the event and thereby increase the chances for cryptotephra detection. As a result, the samples have a sub-annual to annual resolution.

Centrifuging Samples. The ice samples were placed into individual 250ml Nalgene bottles and melted at room temperature. Samples were then gradually decanted into 15ml centrifuge tubes and centrifuged at 2500 rpm for 5 minutes to concentrate the particles at the bottom of the tube. The excess meltwater from these samples was then removed by pipette until ~1ml of water remained. These steps were repeated until all of the meltwater had been transferred from the Nalgene bottles. The bottles were then rinsed twice with ~13ml of deionised water which was then transferred to the tubes and centrifuged. This was to prevent any particles remaining in the bottle.

Mounting Samples. Acrylic discs with a 1cm diameter pre-drilled hole in the centre (total diameter 2.5cm), were covered with Kapton tape at the base and placed upon aluminium platters on top of a hotplate. The concentrated 1ml water samples were then gradually pipetted into the holes and left to evaporate at 60°C. When the samples had completely evaporated, the hotplate was switched off and the samples were left to cool for 1 hour. Buehler EpoThinTM Epoxy resin was prepared by slowly mixing hardener and resin, which was then placed into a desiccator and brought under vacuum for 3 minutes to eliminate bubbles. The resin was then slowly used to backfill the hole, covering the sample using a wooden stick. Care was taken to ensure that a dome did not form on the top of the sample. Samples were then left to cure for 72 hours at room temperature.

Identification of tephra and polishing. After the samples had cured, the Kapton tape was removed and placed on a separate labelled slide. All samples were checked for the presence of tephra using a polarising microscope at x40 magnification. Samples where tephra was identified were prepared for geochemical analysis by polishing the epoxy surface and tephra shards using a 1µm and ¼µm diamond paste for ~10 minutes. This was in order to create a flat surface for geochemical analysis.

B) *Summary of the proximal tephra sample preparation methodology for geochemical analysis at the University of Bern adopted within this study.*

Sampling. Proximal material for the candidate events was obtained from fieldwork in Iceland, with sampling locations selected based on previous published work [1,2,3,4] (see Supplementary Table 4 and Supplementary Figures 10 and 11). Soil sections were exposed, cleaned, logged, and photographed, and the candidate tephra layers were sampled (~10g of each sample obtained) and placed into labelled bags and sealed. Samples were subsequently transported back to the University of Bern, Switzerland.

Lab preparation. ~2 g of each sample were transferred from the labelled bags into labelled centrifuge tubes. The samples were then crushed until they were a fine powder. Once all samples were transferred and crushed, each centrifuge tube was filled with ~14 ml of deionised water. Each sample was subsequently sieved between 125µm and 25µm, and the retained residue transferred to separate centrifuge tubes for each size fraction. These were then filled with ~14 ml of deionised water and centrifuged at 2500 rpm for 5 minutes to concentrate the particles at the bottom of the tube. This was done in a clean environment, one sample at a time, to avoid cross-contamination. The smallest size fraction (25-63 µm) was selected for analysis as it was closest in size range to the ice core tephra samples.

0.25ml of the concentrated sample was pipetted into the 1cm hole of the pre-drilled acrylic discs which were covered with Kapton tape at the base and placed upon aluminium platters on top of a hotplate and left to evaporate at 60°C. When the samples had completely evaporated, the hotplate was switched off and the samples were left to cool for 1 hour. Buehler EpoThinTM Epoxy resin was prepared by slowly mixing hardener and resin, which was then placed into a desiccator and brought under vacuum for 3 minutes to eliminate bubbles. Resin was then used to slowly backfill the hole and cover the sample using a wooden stick. Care was taken to ensure that a dome did not form on the top of the sample. Samples were then left to cure for 72 hours at room temperature.

Polishing. After the samples had cured, the Kapton tape was removed and placed on a separate labelled slide. Samples were prepared for geochemical analysis by polishing the epoxy surface and tephra shards using a 1µm and ¼µm diamond paste for ~10 minutes. This was in order to create a flat surface for geochemical analysis.

Analysis. Major geochemical data was obtained for all five proximal samples using Electron probe microanalysis (EPMA) at the Institute of Geological Sciences, University of Bern, Switzerland. Additional trace element analyses were obtained for three of the five samples (06-752, 05-757, and 04-764) using laser ablation inductively coupled plasma mass spectrometry (LA-ICP-MS) at St Andrews Isotope Geochemistry lab, UK.

II. Supplementary Tables

Ice core	Longitude/Latitude	Elevation m (a.s.l)	Bottom depth (m)	Timespan ([-] BCE/CE)	Accumulation rate (m/yr)	Method (lab)	Parameters analysed	Refs
NGRIP1	75.10°N/42.32°W	2917	1351	187 to 1996	0.19	IC (PICE)	SO_4, Cl-, F-	[5]
NGRIP2	75.10°N/42.32°W	2921	3085	[-]123000 to 1998	0.19	CFA-ICPMS (DRI)	S, Cl, Bi, Tl, Cd, Particles (Part.), H+, conductivity (Cond.)	[6]
NEEM (2011-S1)	77.45°N/51.06°W	2450	410	86 to 2006	0.22	CFA-ICPMS (DRI)	S, Cl, Bi, Tl, Cd, H+,	[7]
TUNU2013	78.04°N/33.88°W	2105	213	280 to 2013	0.1	CFA-ICPMS (DRI)	Cond., tephra(UniBE)	[8]
B19	78.00°N/36.40°W	2234	150.4	748 to 1993	0.1	CFA-ICPMS (DRI)	S, Cl, Bi, Tl, Cd, Br, Part., H+, Cond., tephra(UniBE)	[9]; *This study*
EGRIP	75.38°N/35.60°W	2458	2664	>100000 to 2015**	0.11	IC (AWI)	SO_4, Cl-, F-	[10]; *This study*
RECAP	71.3°N/26.7°W	2315	562.13	[-]118834 to 2013	0.45	CFA-ICPMS (DRI)	S, Cl, Bi, Tl, Cd, Br, Part., tephra(PICE)	[11]; *This study*

Supplementary Table 1: Summary of ice cores utilised in this study including longitude/latitude, elevation, bottom depth, timespan, and accumulation rate. Analysed parameters which were used from each ice core within this study are shown, along with the lab where the measurements were undertaken, unless otherwise indicated. Lab abbreviations: AWI = Alfred-Wegner Institute, Germany; UniBE = University of Bern, Switzerland; DRI = Desert Research Institute, USA; Edin = University of Edinburgh, UK; PICE = Physics of Ice, Climate and Earth, Denmark; QUB = Queen's University Belfast, UK; StAiG = University of St Andrews, UK. **Dating of EGRIP ice core ongoing, with estimated basal age >100 ka at time of submission.

Event	Diagnostic Parameter	Age NS1-2011 and stated uncertainty (CE) for NEEM-2011-S1	Age DRI_NGRIP2 and stated uncertainty (CE) for NGRIP2	Mean Age (CE)	Corresponding date from other proxy or documentary sources
Volcanic eruption 626	Sulfur increase	626 (±0)	625 (±2)	626	Documentary records of volcanic dust veil starting in October 626 [8]
Onset Hrafnkatla Episode	Thallium increase	752 (±1)	750 (±2)	751	None
End Hrafnkatla Episode	Thallium decrease	764 (±1)	762 (±2)	763	Strong winter climate anomalies in Europe and Black Sea culminating in winter 763/764 [12]
Solar proton event 774	^{10}Be increase	774 (±0)	773 (±2)	774	June to August 774, based on seasonally resolved 14C data from an interhemispheric tree-ring network [13]
Volcanic eruption 800	Short-lived sulfur spike	800 (±1)	799 (±2)	800	Strong NH summer cooling in various tree-ring reconstructions in 800 [14,15]
Eldgjá eruption 939-940	Sulfur increase	939 (±0)	939 (±2)	939	Documentary records of volcanic dust veil starting in 939 [7] and major tree-ring cooling in 940; Nile summer flood failure in 939 [16]

Supplementary Table 2: Key dates in two independent ice-core chronologies from Greenland, NS1-2011[8], and DRI_NGRIP2[6] the latter being identical with GICC21 between 681 and 1270 CE[17]. Between 626 and 800 CE, DRI-NGRIP2 is within error identical with NS1-2011 but is consistently older by 1 to 2 years relative to NS1-2011 and relative to specific marker horizons identified in tree-ring and documentary records.

Event	Diagnostic Parameter	Age NS1-2011 and stated uncertainty (CE) for NEEM-2011-S1	Age DRI_NGRIP2 and stated uncertainty (CE) for NGRIP2	Age GICC21 and stated uncertainty (CE) for NGRIP2	Mean Age (CE)	Corresponding date from other proxy or documentary sources
Volcanic eruption 626	Sulfur increase	626 (±0)	625 (±2)	626 (±4)	626	Documentary records of volcanic dust veil starting in October 626 [8]
Onset Hrafnkatla Episode	Thallium increase	752 (±1)	750 (±2)	750 (±4)	751	None
End Hrafnkatla Episode	Thallium decrease	764 (±1)	762 (±2)	762 (±4)	763	Strong winter climate anomalies in Europe and Black Sea culminating in winter 763/764 [12]
Solar proton event 774	^{10}Be increase	774 (±0)	773 (±2)	773 (±4)	773	June to August 774, based on seasonally resolved 14C data from an interhemispheric tree-ring network [13]
Volcanic eruption 800	Short-lived sulfur spike	800 (±1)	799 (±2)	799 (±4)	799	Strong NH summer cooling in various tree-ring reconstructions in 800 [14,15]
Eldgjá eruption 939-940	Sulfur increase	939 (±0)	939 (±2)	939 (±4)	939	Documentary records of volcanic dust veil starting in 939 [8] and major tree-ring cooling in 940; Nile summer flood failure in 939 [16]

Supplementary Table 3: Key dates in three ice-core chronologies from Greenland, NS1-2011[8], DRI_NGRIP2[6], and GICC21[17].

Sample ID	Site	Longitude	Latitude	Event (Age CE)	Volcanic system(s)	Depth (cm)		Description (in field)
						Bottom	*Top*	
06-752	Atley, Iceland	18.68231°W	63.67295°N	Hrafnkatla (763)	Katla	65	49	39-41 cm fa-ml, individual beds of ash dominated and lapilli dominated beds
05-757	Atley, Iceland	18.68231°W	63.67295°N	Hrafnkatla (763)	Katla	49	38	
04-764	Atley, Iceland	18.68231°W	63.67295°N	Hrafnkatla (763)	Katla	38	26	
01-SL	Atley, Iceland	18.68231°W	63.67295°N	Settlement Layer (877)	Torfajökull & Bárdarbunga–Veidivötn	9	0	8-9 cm thick greenish grey tephra, fa-ca
13-SL-877	Quarry Hafid, Iceland	19.786°W	64.054°N	Settlement Layer (877)	Torfajökull & Bárdarbunga–Veidivötn	35	33	2 cm light tephra to lapilli

Supplementary Table 4: Summary table of proximal samples obtained as part of this study. Including, sample ID, sampling location, corresponding event, volcanic system, and description of the layer. Abbreviations used in the field description are as follows: f/m/ca or l, fine/medium/coarse ash or lapilli. Annotated photographs of the soil sections for Atley and Quarry Hafid can be found in Supplementary Figure 11.

III. Supplementary Figures

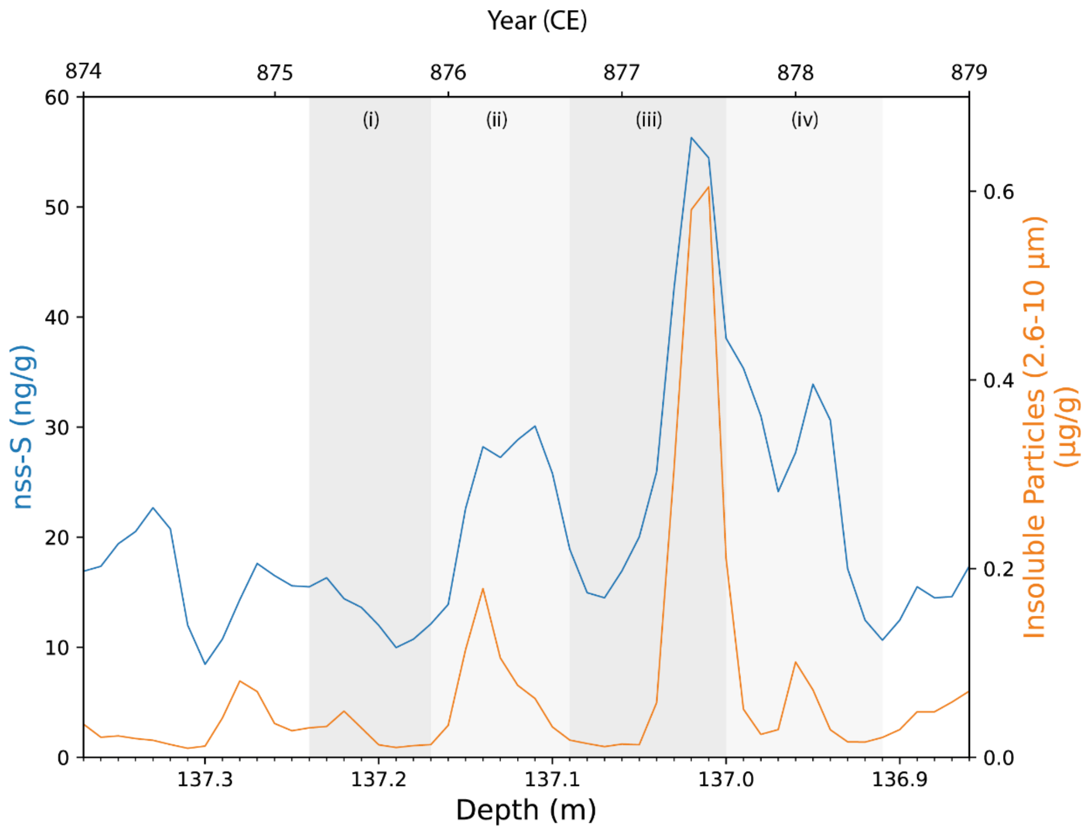

Supplementary Figure 1: Example of targeted sampling approach adopted within this study. The non-sea-salt sulfur (nss-S) and insoluble particle records from the B19 ice core are shown. Grey bars denote depth interval and time-span of samples. In this example, two background samples (i; 137.24-137.16m) and (iv; 136.99-136.91m), were taken alongside samples which isolated peaks in insoluble particles, which coincided with peaks in nss-S - (ii; 137.16-137.08m) and (iii; 137.08-136.99m). Tephra glass shards were successfully identified in sample period (iii), and have been geochemical attributed to the Settlement Layer, Iceland (B19_137.08m_877CE).

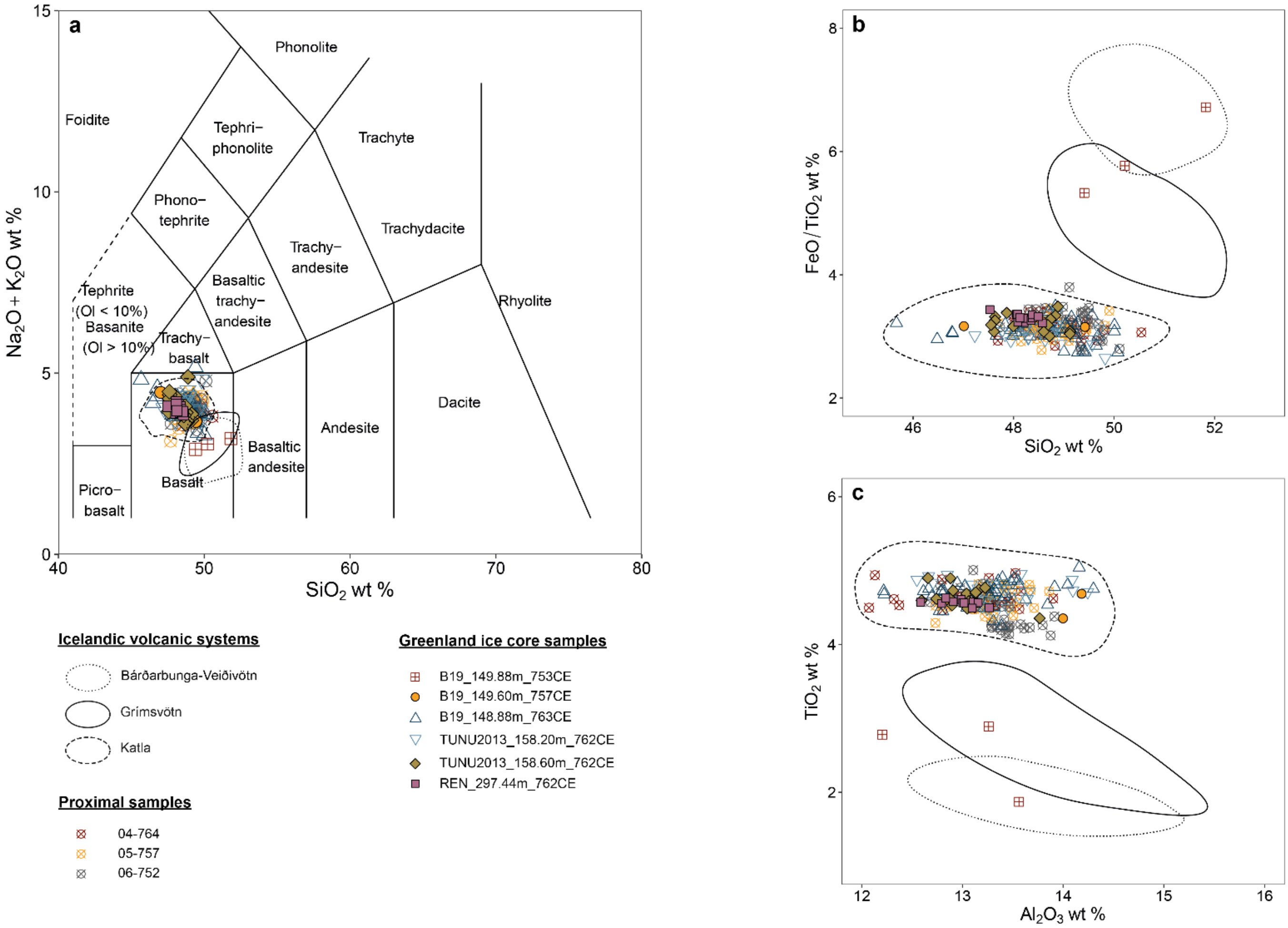

Supplementary Figure 2: (a) Major element glass shard analyses from the 751–763 CE event cryptotephra deposits from the B19, TUNU2013, and RECAP ice cores and proximal correlatives obtained as part of this study (see Supplementary Data) plotted based on magmatic composition- Total Alkali ($Na_2O + K_2O$) vs Silica (SiO_2) [18] and major element bi-plots of (b) FeO/TiO_2 vs SiO_2 and (c) TiO_2 vs Al_2O_3. Geochemical fields for the Grímsvötn, Katla, and Bárðarbunga-Veiðivötn Icelandic volcanic systems have been constructed based on published data ([1,19,20,21,22,23,24,25,26,27,28,29]). All data have been normalised to 100 % (anhydrous basis).

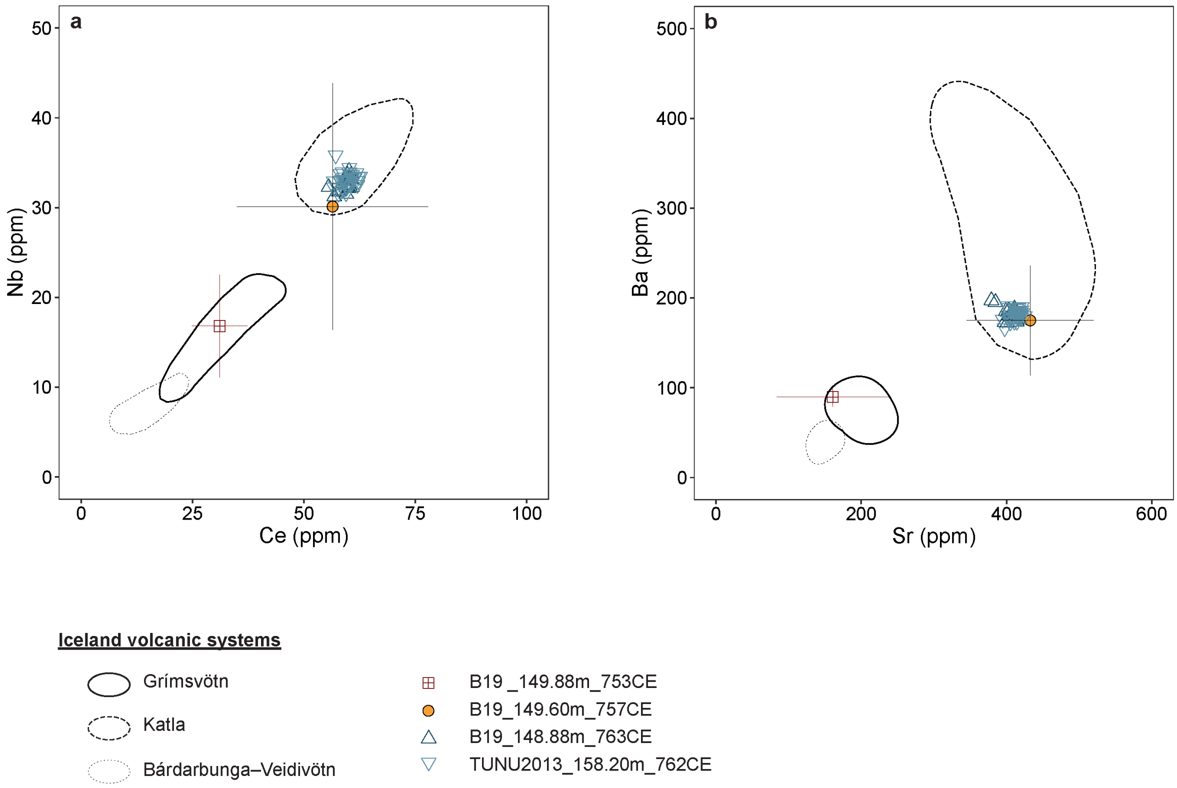

Supplementary Figure 3: Trace element bi-plots (a) Nb vs Ce and (b) Ba vs Sr for 751—763 CE event cryptotephra deposits from B19 and TUNU2013 ice cores, based on absolute concentrations (ppm) from single grains. Geochemical fields for the Grímsvötn, Katla, and Bárdarbunga–Veidivötn Icelandic volcanic systems have been constructed based on published data ([29,30,31,32,33,34,35]) and proximal analyses obtained in this study (see Supplementary Data). Error bars represent 2σ standard deviation of individual analyses in relation to the ML3B reference glass.

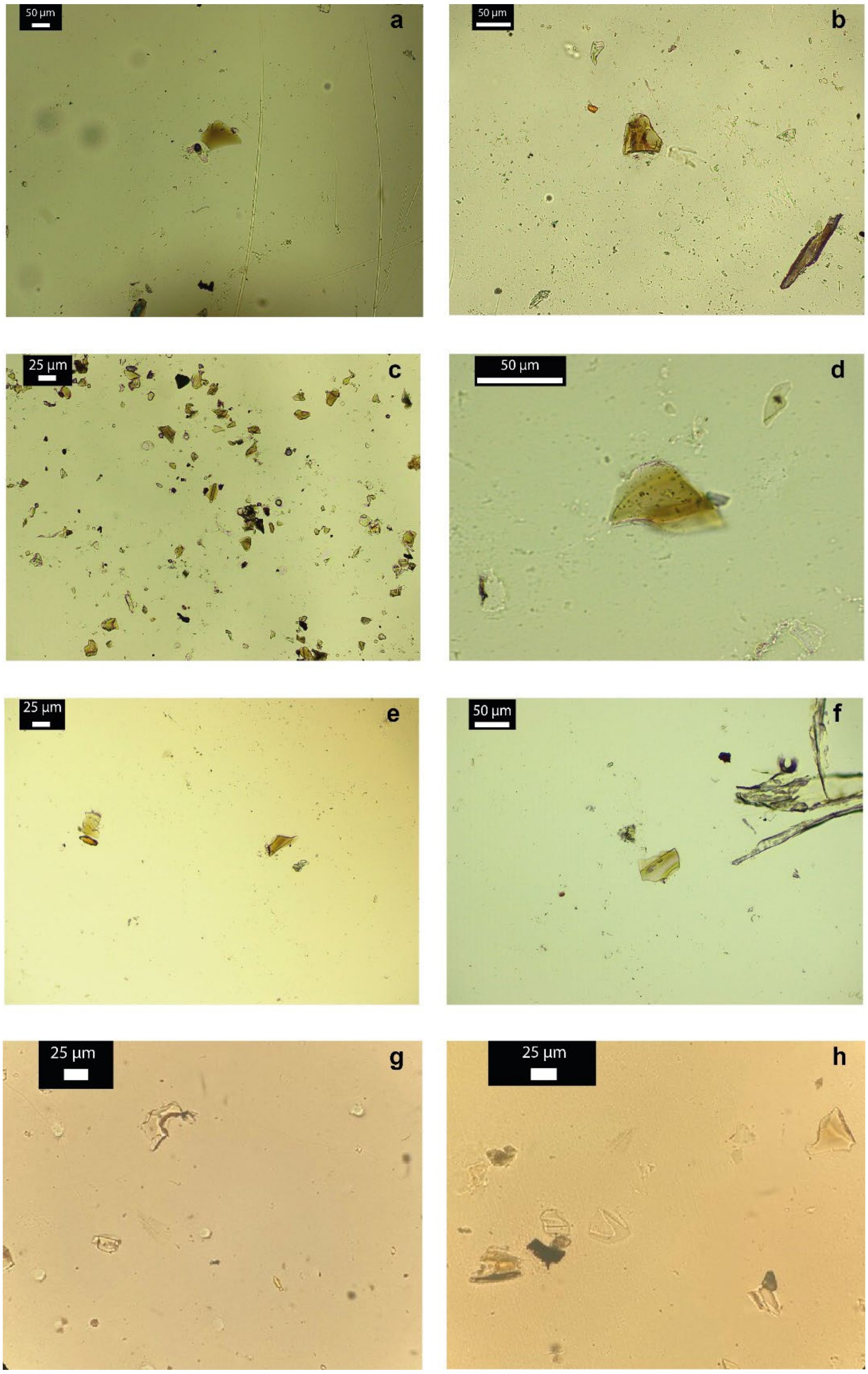

Supplementary Figure 4: Photographs of glass shards identified in Greenland ice core samples within this study; (a) B19_149.88m_753CE (Grímsvötn, Iceland); (b) B19_149.60m_757CE (Katla, Iceland); (c, d) B19_148.88m_763CE and TUNU2013_158.2m_762CE (e, f) (Hrafnkatla volcanic eruption, Katla, Iceland); (g) B19_147.29m_781CE (Grímsvötn, Iceland); and (h) B19_137.08m_877CE (Settlement Layer, Bárdarbunga–Veidivötn and Torfajökull, Iceland).

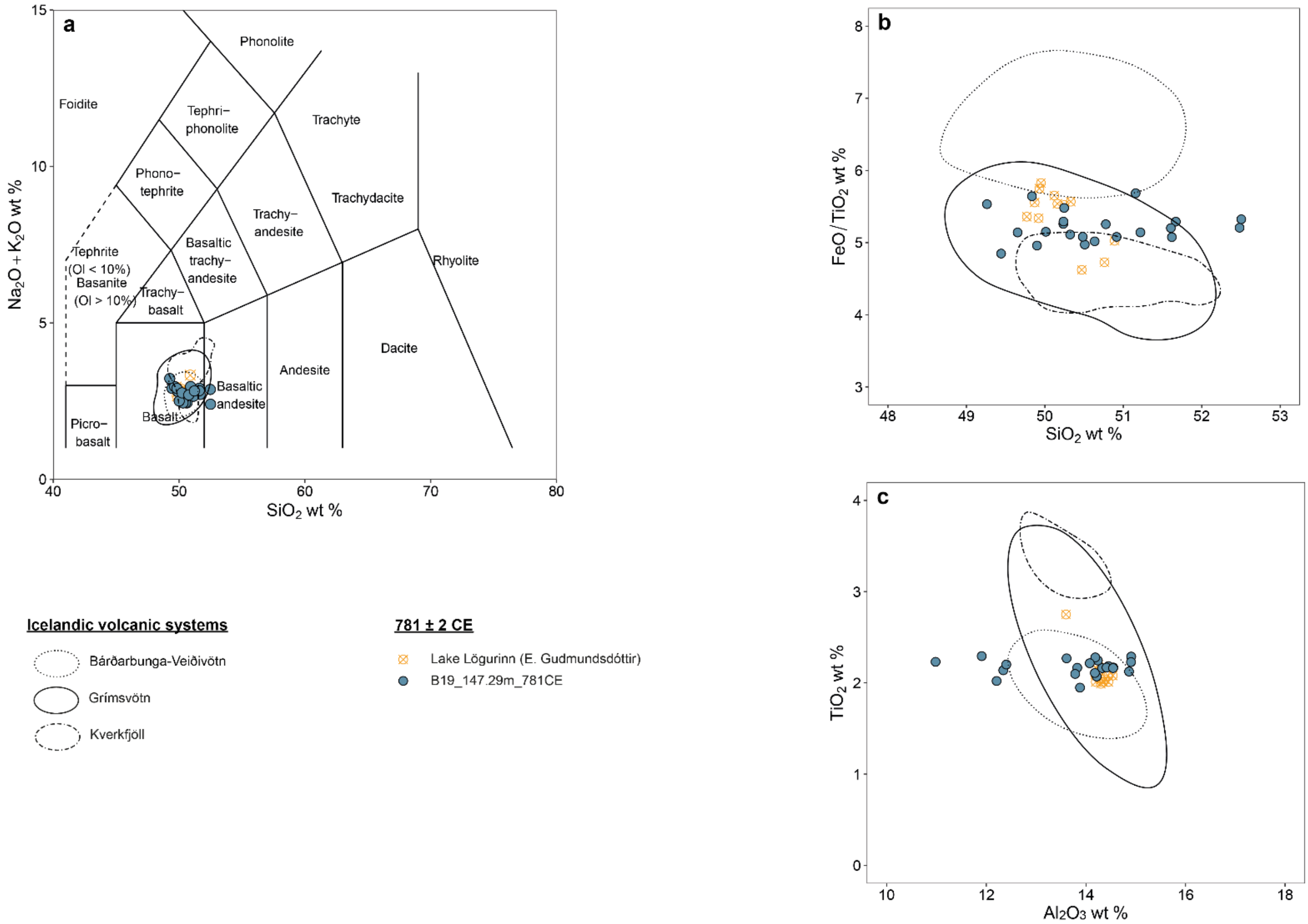

Supplementary Figure 5: (a) Major element glass shard analyses from the 781 ± 2 CE event cryptotephra deposits from the B19 ice core plotted based on magmatic composition- Total Alkali ($Na_2O + K_2O$) vs Silica (SiO_2) [18] alongside existing analyses from an associated horizon in lake Lögurinn, Iceland (Pers. Comm. E. Gudmundsdóttir). Major element bi-plots (b) FeO/TiO_2 vs SiO_2 and (c) TiO_2 vs Al_2O_3. Geochemical fields for the Bárdarbunga–Veidivötn, Grímsvötn, and Kverkfjöll Icelandic volcanic systems have been constructed based on published data ([1,20,21,22,23,24,25,26,27,29,36]). All data have been normalised to 100 % (anhydrous basis).

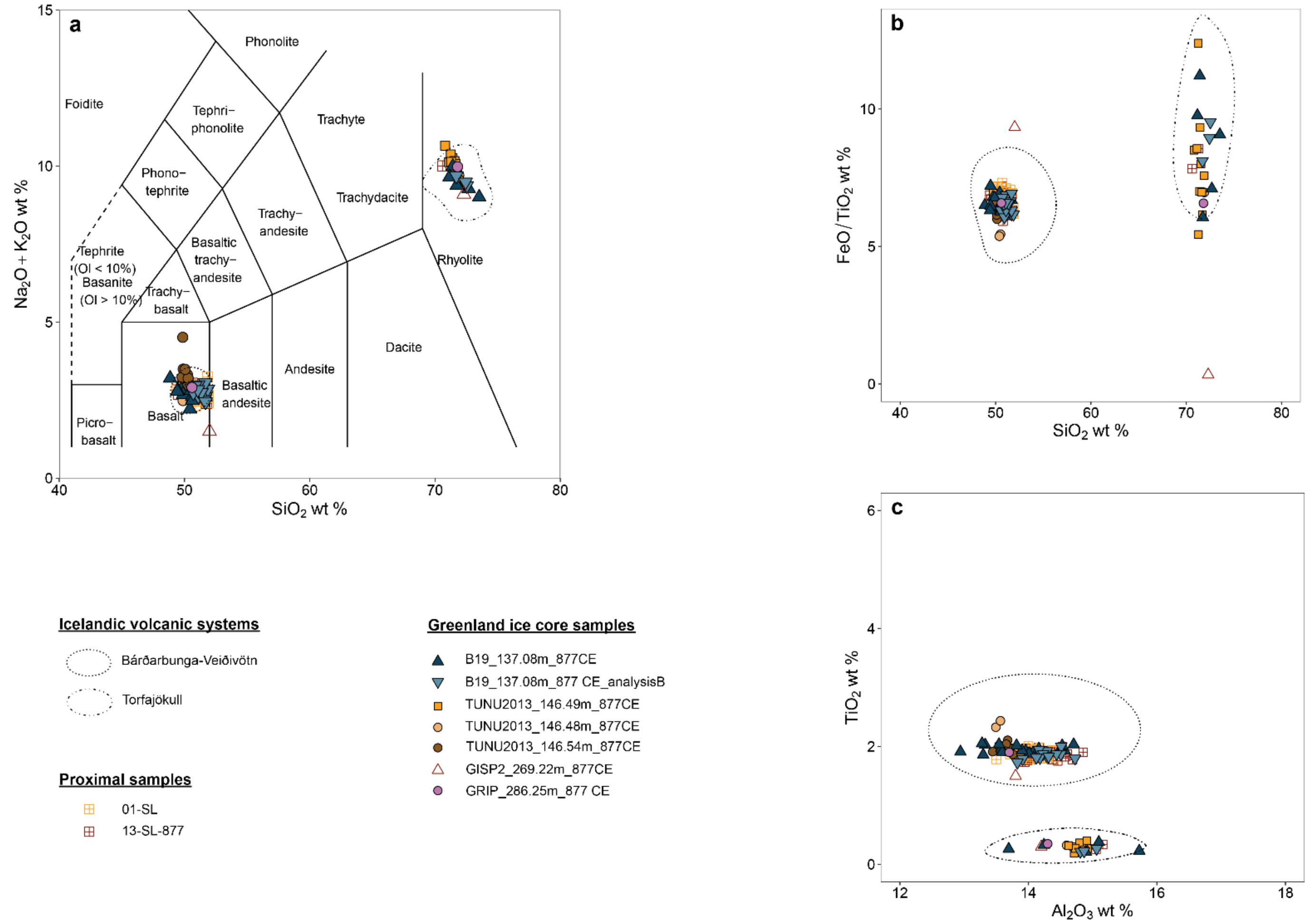

Supplementary Figure 6: (a) New major element glass shard analyses from the 877 CE event cryptotephra deposits from the B19 and TUNU2013 ice cores plotted based on magmatic composition – Total Alkali (Na_2O + K_2O) vs Silica (SiO_2) [18] alongside published ice core analyses (GRIP [37], GISP2 [38], TUNU2013 [39]) and proximal material from the same event collected as part of this study (see Supplementary Data). Major element bi-plots are shown in (b) FeO/TiO_2 vs SiO_2 and (c) TiO_2 vs Al_2O_3. Geochemical fields for the Bárdarbunga–Veidivötn, Torfajokull Icelandic volcanic systems have been constructed based on published data ([1,20,22,24,25,26,27,40,41]). All data have been normalised to 100 % (anhydrous basis).

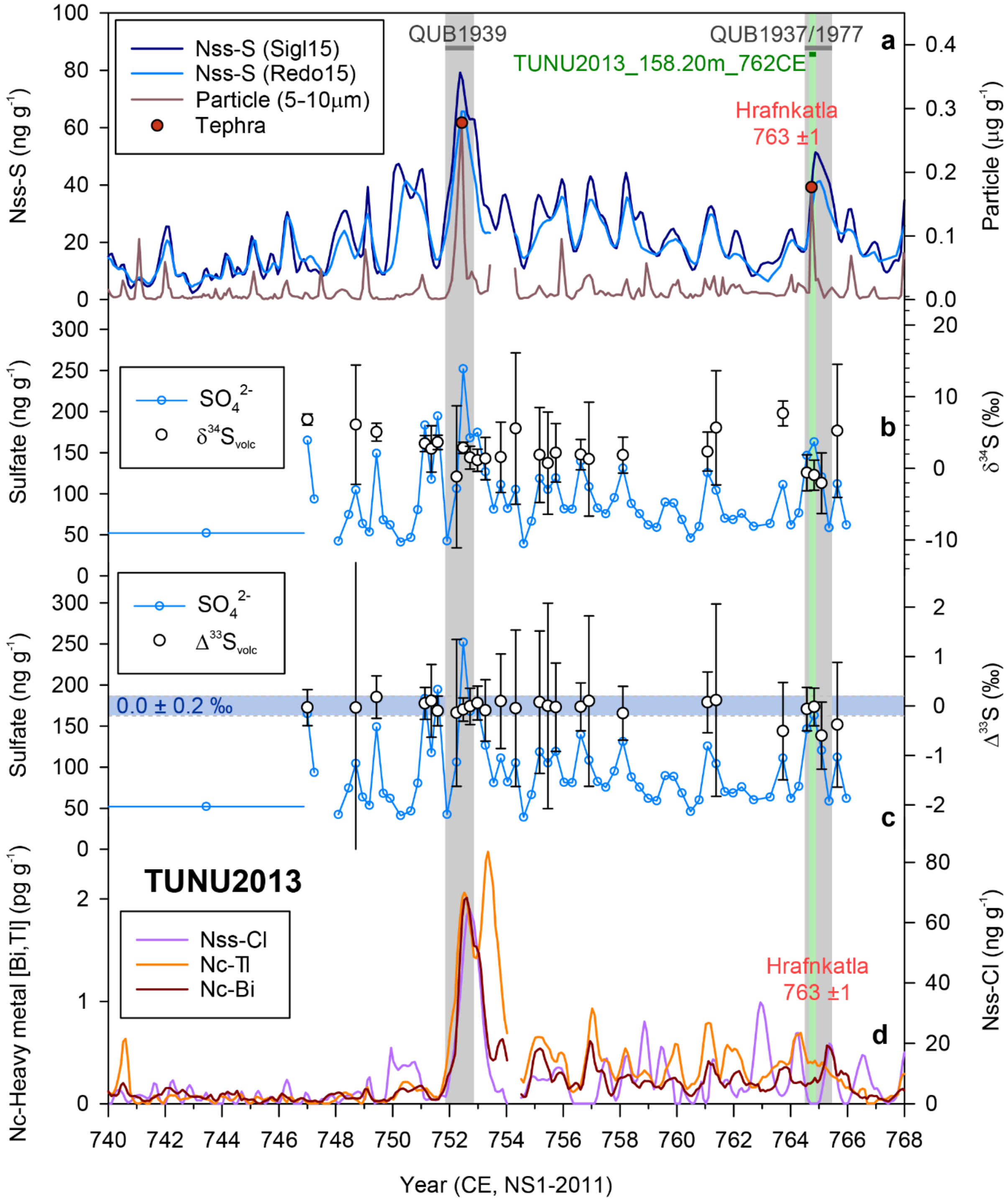

Supplementary Figure 7: (a) Non-sea-salt Sulfur (Nss-S) from TUNU2013 ice core and associated insoluble particle record (5–10 µm) across the period 742–768 CE. Targeted tephra sample (grey) and sulfur isotope (green) locations (which were screened for tephra) are shown, with the geochemically confirmed occurrences of cryptotephra indicated by red circles; (b) Background corrected $\delta^{34}S$ (‰) and sulfur concentrations versus time recorded in the TUNU2013 ice core; (c) Background corrected $\Delta^{33}S$ (‰) and sulfur concentrations versus time recorded in the TUNU2013 ice core. Blue shading indicates stratospheric $\Delta^{33}S$ range (0.0 ± 0.2 ‰); (d) non-crustal thallium (Nc-Tl), non-crustal bismuth (Nc-Bi) and non-sea-salt chlorine (Nss-Cl) record for TUNU2013 ice core. A pronounced enrichment can be observed at the beginning of the Hrafnkatla episode.

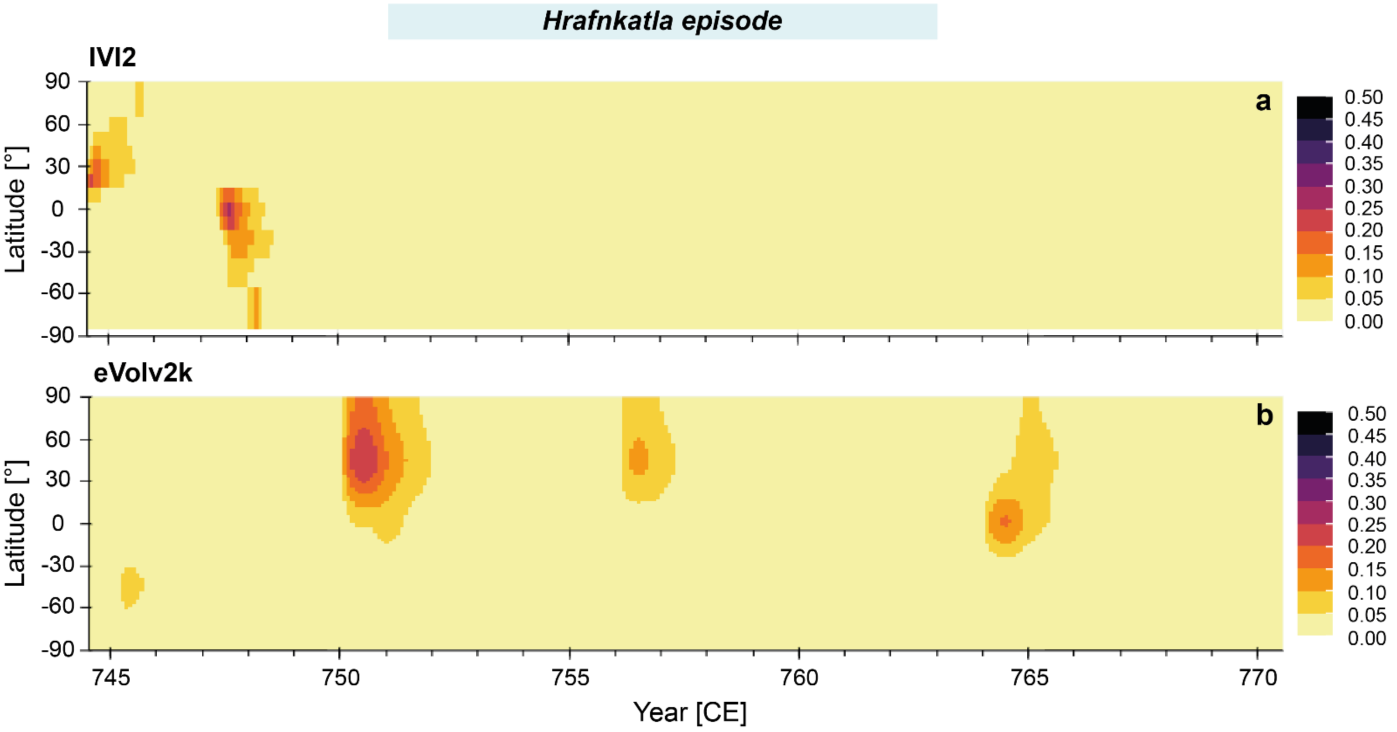

Supplementary Figure 8: a) IVI2[42] and b) eVolv2k[43] Stratospheric Aerosol Optical Depth (SAOD) estimates based on polar ice core records across the period 745—770 CE. No volcanic events were detected in the IVI2 estimates across the Hrafnkatla episode, in contrast to eVolv2k where some volcanic perturbations were incorporated. Data was plotted using the SAOD Visualization App (https://cj.argpages.usask.ca/saod-visualization/) Ogilvie, C.J. [2022][44].

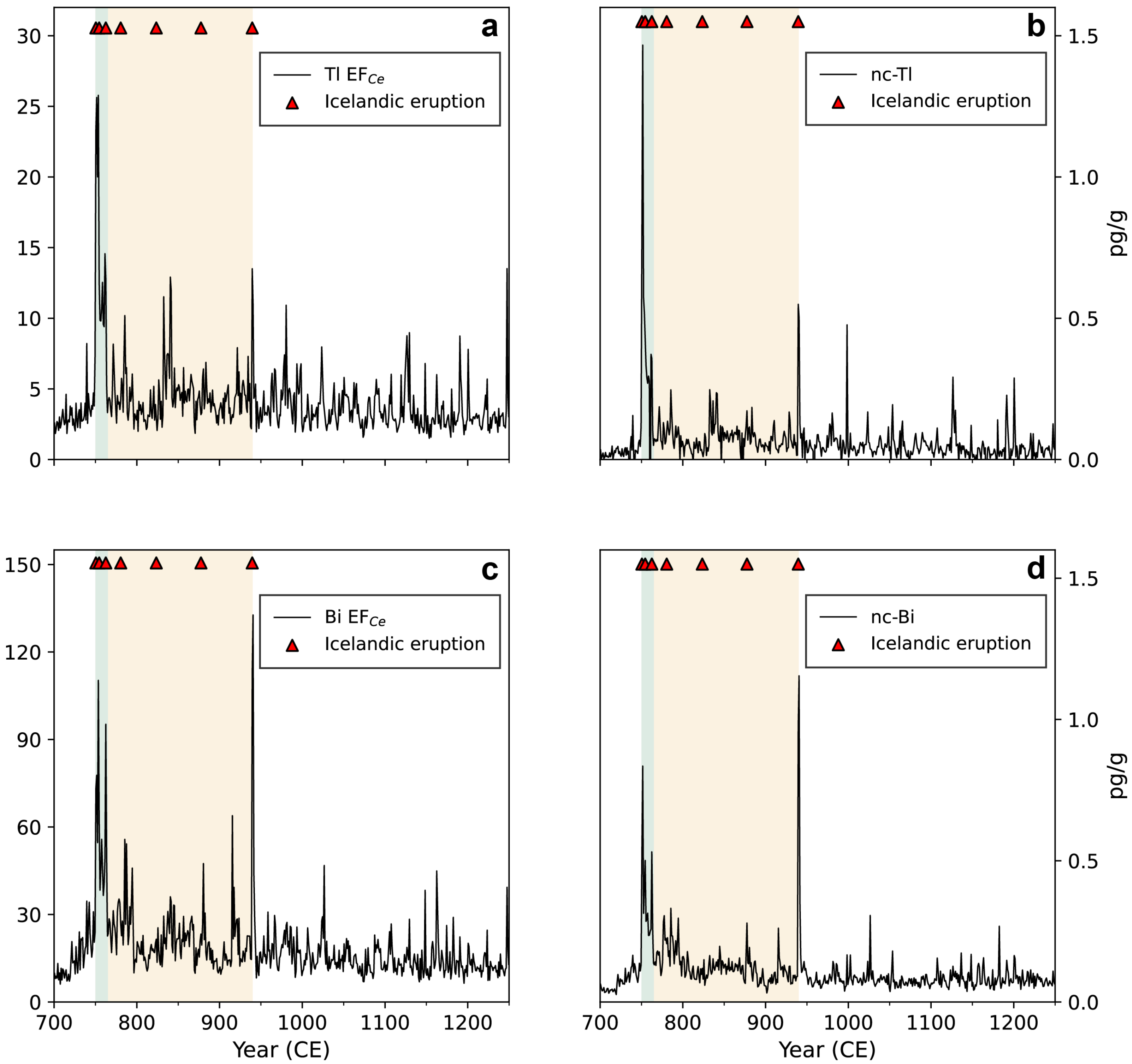

Supplementary Figure 9: a) Enrichment Factor of Tl relative to Ce (a crustal dust tracer) defined as EF =([Tl]ice/[Ce]ice) / ([Tl]crust/[Ce]crust) with crustal values from McLennan (2001)[45]; b) non-crustal-Tl defined as [Tl] – (0.01172 x [Ce]); c) Enrichment Factor of Bi relative to Ce calculated as for Tl; non-crustal-Bi defined as [Bi] – (0.00198 x [Ce]). All Cerium concentration values were corrected for under-recovery during CFA analysis by multiplying with 1.7 following Arienzo et al.[46]. The Hrafnkatla episode (blue shading) and Icelandic Active period (beige shading) are marked for reference along with confirmed Icelandic volcanic eruptions (red triangles) across the study period 700-1000 CE.

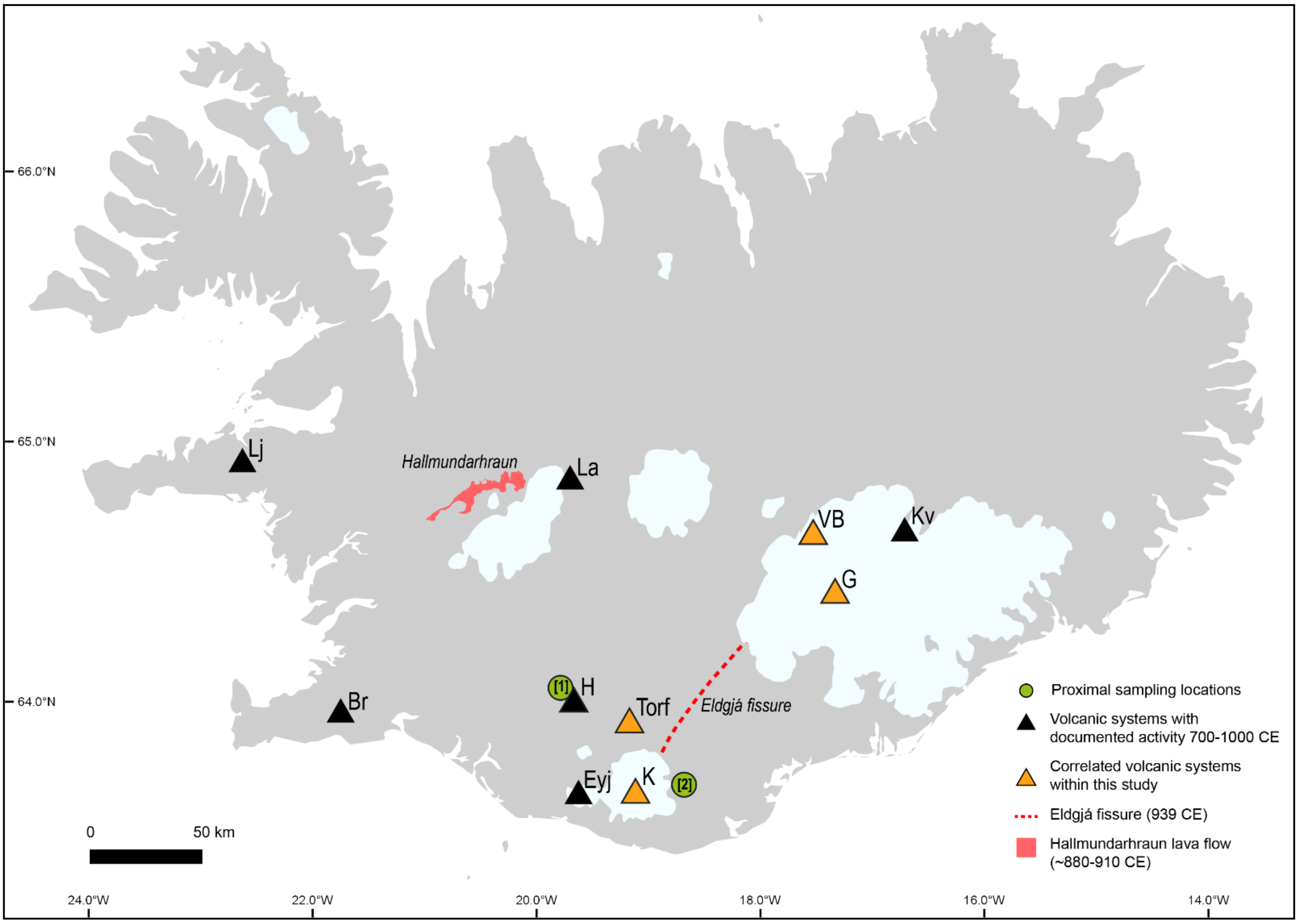

Supplementary Figure 10: Map of Iceland with the location of Icelandic volcanic systems which experienced activity during the period 700-1000 CE (based on published literature [2, 47, 48, 49], the Global Volcanism Program, Smithsonian Institution[50], and the Catalogue of Icelandic volcanoes[51]) indicated by the black triangles, with Lj(Ljósufjöll), Br(Brennisteinsfjöll), La(Oddnýjarhnjúkur-Langjökull), Kv(Kverkfjöll), Eyj(Eyjafjallajökull), and H(Hekla). Icelandic volcanic systems with which a correlation has been made to in this study, K (Katla), G(Grímsvötn), VB(Bárdarbunga–Veidivötn), and Torf(Torfajökull) are indicated by the orange triangles. The ~880–910 CE Hallmundarhraun lava flow, and the Eldgjá fissure, products of the Oddnýjarhnjúkur-Langjökull and Katla volcanic systems respectively are shown. The locations of where proximal samples were obtained for geochemical cryptotephra analysis are indicated by the green circles with (1) Quarry Hafid Outcrop [64.054°N, 19.786°W] and (2) Atley outcrop [63.67295°N, 18.68231°W].

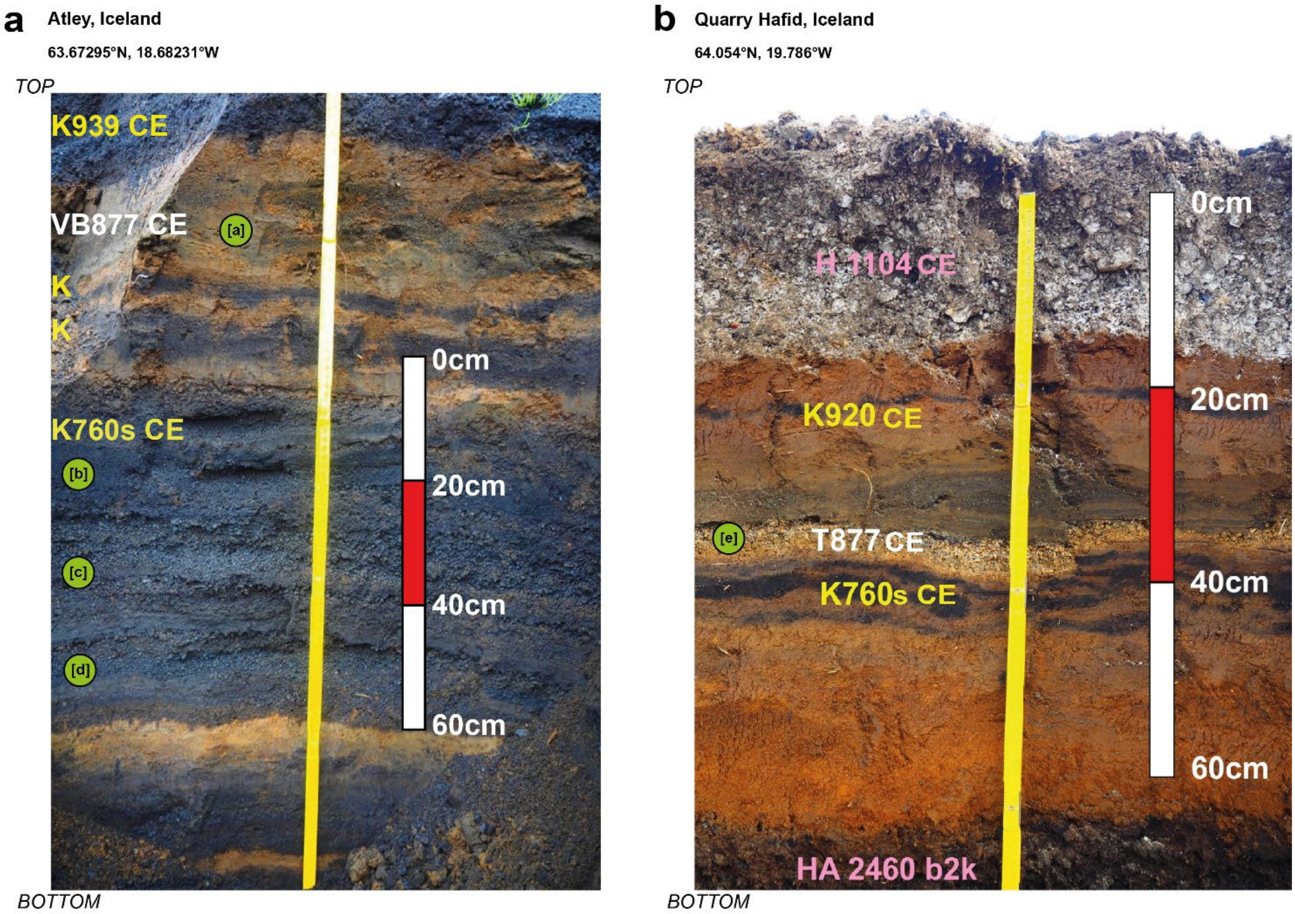

Supplementary Figure 11: (a) Annotated photograph of outcrop at Atley, Iceland. Eruption layers identified are indicated with K939 CE, VB877 CE, and K760s CE being the 939 CE Eldgjá eruption of Katla, the 877 CE Bárdarbunga–Veidivötn component of the Settlement Layer, and the 763 ± 1 CE Hrafnkatla eruption of Katla respectively. K indicates an eruption of Katla, for which no correlation was made in this study. Proximal samples collected as part of this study are shown by the green circles with [a] 01-SL, [b] 04-764, [c] 05-757, and [d] 06-752. A scale bar is provided for reference. (b) Annotated photograph of outcrop at Quarry Hafid, Iceland. Eruption layers identified are indicated with H1104 CE, K920 CE, T877 CE, K760s CE, and HA 2460 b2k being the 1104 CE eruption of Hekla, the 920 CE eruption of Katla, the 877 CE Torfajökull component of the Settlement Layer, the 763 ± 1 CE Hrafnkatla eruption of Katla, and the 1050 BCE eruption of Hekla respectively. The proximal samples collected as part of this study is shown by the green circle with [e] 13-SL877. A scale bar is provided for reference.

IV. Supplementary References

1. Óladóttir, B. A., Larsen, G. & Sigmarsson, O. Holocene volcanic activity at Grímsvötn, Bárdarbunga and Kverkfjöll subglacial centres beneath Vatnajökull, Iceland. *Bull. Volcanol.* **73**, 1187–1208 (2011).

2. Óladóttir, B. A., Larsen, G. & Sigmarsson, O. Volume estimates of nine Katla tephra layers. *Jökull.* **64**, 23–40 (2014).

3. Óladóttir, B. A., Sigmarsson, O. & Larsen, G. Tephra productivity and eruption flux of the subglacial Katla volcano, Iceland. *Bull. Volcanol.* **80**, 1–16 (2018).

4. Óladóttir, B. A., Larsen, G., Thordarson, T. & Sigmarsson, O. The Katla volcano S-Iceland: Holocene tephra stratigraphy and eruption frequency. *Jökull* **55**, 53–74 (2005).

5. Plummer, C. T. *et al.* An independently dated 2000-yr volcanic record from Law Dome, East Antarctica, including a new perspective on the dating of the 1450s CE eruption of Kuwae, Vanuatu. *Clim. Past* **8**,6, 1929–1940 (2012).

6. McConnell, J. R. *et al.* Lead pollution recorded in Greenland ice indicates European emissions tracked plagues, wars, and imperial expansion during antiquity. *Proc. Natl. Acad. Sci.* **115**, 5726–5731 (2018).

7. Sigl, M. *et al.* A new bipolar ice core record of volcanism from WAIS Divide and NEEM and implications for climate forcing of the last 2000 years. *J. Geophys. Res. Atmos.* **118**, 1151–1169 (2013).

8. Sigl, M. *et al.* Timing and climate forcing of volcanic eruptions for the past 2,500 years. *Nature* **523**, 543–549 (2015).

9. Weißbach, S. *et al.* Spatial and temporal oxygen isotope variability in northern Greenland-implications for a new climate record over the past millennium. *Clim. Past* **12**, 171–188 (2016).

10. Erhardt, T. *et al.* High-resolution aerosol data from the top 3.8 kyr of the East Greenland Ice coring Project (EGRIP) ice core. *Earth Syst. Sci. Data* **15**, 5079–5091 (2023).

11. Simonsen, M. F. *et al.* East Greenland ice core dust record reveals timing of Greenland ice sheet advance and retreat. *Nat. Commun.* **10**, 4494, 10.1038/s41467-019-12546-2 (2019).

12. Newfield, T. P. The contours, frequency and causation of subsistence crises in Carolingian Europe (750-950 CE). in *In Crisis alimentarias en la edad media: Modelos, explicaciones y representaciones* 117–172 (2013).

13. Büntgen, U. *et al.* Multi-proxy dating of Iceland's major pre-settlement Katla eruption to 822–823 CE. *Geology* **45**, 783–786 (2017).

14. Schneider, L. *et al.* Revising midlatitude summer temperatures back to AD 600 based on a wood density network. *Geophys. Res. Lett.* **42**, 4556–4562 (2015).

15. Wilson, R. *et al.* Last millennium northern hemisphere summer temperatures from tree rings: Part I: The long term context. *Quat. Sci. Rev.* **134**, 1–18 (2016).

16. Oppenheimer, C. *et al.* The Eldgjá eruption: timing, long-range impacts and influence on the Christianisation of Iceland. *Clim. Change* **147**, 369–381 (2018).

17. Sinnl, G. *et al.* A multi-ice-core, annual-layer-counted Greenland ice-core chronology for the last 3800 years: GICC21. *Clim. Past* **18**, 1125–1150 (2022).

18. Bas, M. L., Maitre, R. L., Streckeisen, A., Zanettin, B. & Rocks, I. S. on the S. of I. A chemical classification of volcanic rocks based on the total alkali-silica diagram. *J. Petrol.* **27**, 745–750 (1986).

19. Davies, S. M., Turney, C. S. & Lowe, J. J. Identification and significance of a visible, basalt-rich Vedde Ash layer in a Late-glacial sequence on the Isle of Skye, Inner Hebrides, Scotland. *J. Quat. Sci. Publ. Quat. Res. Assoc.* **16**, 99–104 (2001).

20. Larsen, D. J., Miller, G. H., Geirsdóttir, Á. & Thordarson, T. A 3000-year varved record of glacier activity and climate change from the proglacial lake Hvítárvatn, Iceland. *Quat. Sci. Rev.* **30**, 2715–2731 (2011).

21. Wastegård, S. & Davies, S. M. An overview of distal tephrochronology in northern Europe during the last 1000 years. *J. Quat. Sci. Publ. Quat. Res. Assoc.* **24**, 500–512 (2009).

22. Davies, S. M., Elmquist, M., Bergman, J., Wohlfarth, B. & Hammarlund, D. Cryptotephra sedimentation processes within two lacustrine sequences from west central Sweden. *The Holocene* **17**, 319–330 (2007).

23. Jennings, A. *et al.* Holocene tephra from Iceland and Alaska in SE Greenland shelf sediments. *Geol. Soc.*

London, Spec. Publ. **398**, 157–193 (2014).

24. Lawson, I. T. *et al.* Environmental impacts of the Norse settlement: palaeoenvironmental data from Myvatnssveit, northern Iceland. *Boreas* **36**, 1–19 (2007).

25. Watson, E. J., Swindles, G. T., Lawson, I. T. & Savov, I. P. Do peatlands or lakes provide the most comprehensive distal tephra records? *Quat. Sci. Rev.* **139**, 110–128 (2016).

26. Streeter, R. & Dugmore, A. Late-Holocene land surface change in a coupled social–ecological system, southern Iceland: a cross-scale tephrochronology approach. *Quat. Sci. Rev.* **86**, 99–114 (2014).

27. Harning, D. J., Thordarson, T., Geirsdóttir, Á., Zalzal, K. & Miller, G. . Provenance, stratigraphy and chronology of Holocene tephra from Vestfirðir, Iceland. *Quat. Geochronol.* **46**, 59–76 (2018).

28. Wastegård, S. Early to middle Holocene silicic tephra horizons from the Katla volcanic system, Iceland: New results from the Faroe Islands. *J. Quat. Sci.* **17**, 723–730 (2002).

29. Óladóttir, B. A., Sigmarsson, O., Larsen, G. & Devidal, J. L. Provenance of basaltic tephra from vatnajökull subglacial volcanoes, iceland, as determined by major- and trace-element analyses. *The Holocene* **21**, 1037–1048 (2011).

30. Macpherson, C. G., Hilton, D. R., Day, J. M., Lowry, D. & Grönvold, K. High-3He/4He, depleted mantle and low-δ18O, recycled oceanic lithosphere in the source of central Iceland magmatism. *Earth Planet. Sci. Lett.* **223**, 411–427 (2005).

31. Sigmarsson, O., Karlsson, H. R. & Larsen, G. The 1996 and 1998 subglacial eruptions beneath the Vatnajökull ice sheet in Iceland: contrasting geochemical and geophysical inferences on magma migration. *Bull. Volcanol.* **61**, 468–476 (2000).

32. Wood, D. A., Joron, J. L., Treuil, M., Norry, M. & Tarney, J. Elemental and Sr isotope variations in basic lavas from Iceland and the surrounding ocean floor: The nature of mantle source inhomogeneities. *Contrib. to Mineral. Petrol.* **70**, 319–339 (1979).

33. Lacasse, C. *et al.* Bimodal volcanism at the Katla subglacial caldera, Iceland: insight into the geochemistry and petrogenesis of rhyolitic magmas. *Bull. Volcanol.* **69**, 373–399 (2007).

34. Lane, C. S. *et al.* Was the 12.1 ka Icelandic Vedde Ash one of a kind? *Quat. Sci. Rev.* **33**, 87–99 (2012).

35. Tomlinson, E. L. *et al.* Petrogenesis of the Sólheimar ignimbrite (Katla, Iceland): Implications for tephrostratigraphy. *Geochim. Cosmochim. Acta* **86**, 318–337 (2012).

36. Larsen, G. & Eiríksson, J. Late Quaternary terrestrial tephrochronology of Iceland - Frequency of explosive eruptions type and volume of tephra deposits. *J. Quat. Sci.* **23**, 109–120 (2008).

37. Grönvold, K. *et al.* Ash layers from Iceland in the Greenland GRIP ice core correlated with oceanic and land sediments. *Earth Planet. Sci. Lett.* **135**, 149–155 (1995).

38. Zielinski, G. A., Mayewski, P. A., Meeker, L. D., Whitlow, S. & Twickler, M. S. A 110,000-yr record of explosive volcanism from the GISP2 (Greenland) ice core. *Quat. Res.* **45**, 109–118 (1996).

39. Plunkett, G., Sigl, M., Mcconnell, J. R., Pilcher, J. R. & Chellman, N. J. The significance of volcanic ash in Greenland ice cores during the Common Era. *Quat. Sci. Rev.* **301**, 107936; 10.1016/j.quascirev.2022.107936 (2023).

40. Plunkett, G. & Pilcher, J. R. Defining the potential source region of volcanic ash in northwest Europe during the Mid- to Late Holocene. *Earth-Science Rev.* **179**, 20–37 (2018).

41. Meara, R. H. H., Thordarson, T. H., Pearce, N. J. G., Hayward, C. & Larsen, G. A catalogue of major and trace element data for Icelandic Holocene silicic tephra layers. *J. Quat. Sci.* **35**, 122–142 (2020).

42. Gao, C., Robock, A. & Ammann, C. Volcanic forcing of climate over the past 1500 years: An improved ice core-based index for climate models. *J. Geophys. Res. Atmos.* **113**, D23; 10.1029/2008JD010239 (2008).

43. Toohey, M. & Sigl, M. Volcanic stratospheric sulfur injections and aerosol optical depth from 500 BCE to 1900 CE. *Earth Syst. Sci. Data* **9**, 809–831 (2017).

44. Ogilvie, C.J. SAOD Visualization App. https://cj.argpages.usask.ca/saod-visualization/ (2022).

45. McLennan, S. M. Relationships between the trace element composition of sedimentary rocks and upper continental crust. *Geochemistry, Geophys. Geosystems* **2**,4; 10.1029/2000GC000109 (2001).

46. Arienzo, M. M., McConnell, J. R., Chellman, N. & Kipfstuhl, S. Method for correcting continuous ice-core

elemental measurements for under-recovery. *Environ. Sci. Technol.* **53**, 5887–5894 (2019).

47. Gudmundsdóttir, E.R. Larsen, G., Björck, S., Ingólfsson, Ó. & Striberger, J. A new high-resolution Holocene tephra stratigraphy in eastern Iceland: Improving the Icelandic and North Atlantic tephrochronology. *Quat. Sci. Rev.* **150**, 234–249 (2016).

48. Gudmundsdóttir, E.R. Larsen, G. & Eiríksson, J. Tephra stratigraphy on the North Icelandic shelf: extending tephrochronology into marine sediments off North Iceland. *Boreas* **41**, 719–734 (2012).

49. Óladóttir, B. A., Sigmarsson, O., Larsen, G. & Thordarson, T. Katla volcano, Iceland: magma composition, dynamics and eruption frequency as recorded by Holocene tephra layers. *Bull. Volcanol.* **70**, 475–493 (2008).

50. Global Volcanism Program, Smithsonian Insitution. https://volcano.si.edu/ (2023).

51. Catalogue of Icelandic Volcanoes. https://icelandicvolcanos.is/ (2014).